WORKSPACE CHARACTERIZATION OF PLANAR THREE-LEGGED PLATFORMS WITH HOLONOMIC HIGHER PAIRS

M. J. D. HAYES
Institut für Automation, Montanuniversität Leoben
Peter-Tunner-Strasse 27, A-8700 Leoben, Austria
email: john.hayes@unileoben.ac.at

AND

M. L. HUSTY
Institut für angewandte Geometrie, Montanuniversität Leoben
Peter-Tunner-Strasse 27, A-8700 Leoben, Austria
email: husty@unileoben.ac.at

Abstract. The workspace of planar three-legged platforms with holonomic higher pairs is examined. Kinematic mapping is used to represent distinct displacements of the end-effector as points in a three-dimensional projective image space. The kinematic image of the workspace is shown to be the intersection of solid regions bounded by the envelopes of three families of hyperboloids. The hyperboloids of each family are identical but their axes lie in a ruled surface. The pre-image of the envelopes bounding each solid region consists of pairs of parallel transcendental curves which correspond to the reachable workspace boundary of each leg for one end-effector reference point. An example is given, showing that such platforms can be designed with a large, hole-free dextrous workspace. In this case, the dextrous workspace is on the order of one-third of the reachable workspace.

1. Introduction

Research interest in parallel manipulators has grown steadily over the last twenty-five years. This is partly due to their inherent advantages over serial manipulators where accuracy, stiffness, load-to-weight-ratio and operating speeds are concerned (Merlet, 1999). One major disadvantage of parallel manipulators in general, compared to serial ones, is that their

reachable workspace is small and may contain a high density of interior singularities (Sefrioui and Gosselin, 1992; Collins and McCarthy, 1998; Husty *et al.*, 1999). Although the workspace analysis of planar three-legged manipulators is well established, see Gosselin (1988), Merlet (1990), Husty (1996), for example, work on those containing holonomic higher pairs is rare. In fact, only one paper on this subject was found in the literature, Agrawal and Pandravada (1993), and this offering seems to be incomplete. It has been stated in Hayes *et al.* (1999b) that these manipulators have interesting geometric properties that lead to useful applications. This gives the motivation to carefully study the workspace of these manipulators.

This paper uses kinematic mapping for the purpose of workspace analysis. The method employed is based on that found in Husty (1996), wherein platforms consisting of three revolute-prismatic-revolute (RPR) legs are analyzed. The results presented in this paper can also be applied to a broad sub-class of lower pair three-legged platforms as described in Merlet (1996), Husty *et al.* (1999), Hayes (1999). Because of the illustrative description of all possible positions of the end-effector system as a surface-bound solid region in an image space, it is believed that this is a useful tool for designers. Moreover, it facilitates computations when the reachable workspace of more than one reference point in the end-effector system has to be determined.

2. Manipulator Description

The planar manipulator, shown in Fig. 1, consists of three closed kinematic chains. The circular disk, modelled as a pinion, rolls without slip on each of the three racks tangent to it. We call the kinematic connection between the rack and pinion a *gear* (G) *pair*. It is a *higher* kinematic pair because of the line contact between the two links. Moreover, the rolling constraints are holonomic due to the pure rolling and because the motion is planar. Hence, the constraint equations can be expressed in terms of displacement. Each of the three legs connect a rack to a base point via two *revolute* (R) *pairs*. Each closed chain in the manipulator is an RRGGRR chain.

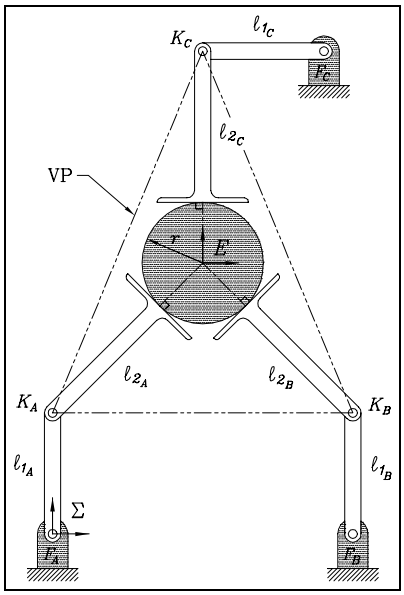

Figure 1. Planar platform.

The leg links are rigid and a rack is rigidly attached to the disk end of each second link. The R-pairs connecting two links in a leg shall be

referred to as *knee joints* K_A, K_B, K_C, and are constrained to move on circles centred on the three points F_A, F_B, F_C, which are grounded to a fixed rigid base. The position and orientation of the pinion end-effector are described by reference frame E, which has its origin on the disk centre and moves with it. Frame Σ has its origin at the base of leg A and is fixed.

The kinematics of these platforms, unlike those of lower-pair jointed three-legged ones, are dependent on the initial assembly configuration (IAC), due to the roll-without-slip condition, see Agrawal and Pandravada (1993), Hayes *et al.* (1999a). This means that changing the IAC will change the workspace. For kinematics computations one reference position can be used as the IAC. We have used the position shown in Fig. 1.

3. A Kinematic Mapping of Planar Displacements

It is convenient to think of the relative planar motion between two rigid bodies as the motion of a Cartesian reference coordinate system E, attached to one of the bodies, with respect to the Cartesian coordinate system Σ, attached to the other. The position of a point in E relative to Σ can be given by the homogeneous linear transformation

$$\begin{bmatrix} X \\ Y \\ Z \end{bmatrix} = \begin{bmatrix} \cos\varphi & -\sin\varphi & a \\ \sin\varphi & \cos\varphi & b \\ 0 & 0 & 1 \end{bmatrix} \begin{bmatrix} x \\ y \\ z \end{bmatrix}, \tag{1}$$

where $(x/z, y/z)$ are the Cartesian coordinates of a point in E, $(X/Z, Y/Z)$ are those of the same point in Σ. The Cartesian coordinates of the origin of E measured in Σ are (a, b). The rotation angle measured from the X-axis to the x-axis is φ, the positive sense being counter-clockwise.

The kinematic mapping used here is discussed in detail by Bottema and Roth (1979), De Sa and Roth (1981) and by Ravani and Roth (1983). The image of the displacement parameters (a, b, φ) under the kinematic mapping is called the *image point*. Distinct displacements have unique image points, given by

$$\begin{aligned} (X_1 : X_2 : X_3 : X_4) = {} & [a\sin(\varphi/2) - b\cos(\varphi/2) : \\ & a\cos(\varphi/2) + b\sin(\varphi/2) : \\ & 2\sin(\varphi/2) : 2\cos(\varphi/2)]. \end{aligned} \tag{2}$$

By virtue of the relationships expressed in Eq. (2), the transformation matrix from Eq. (1) may be expressed in terms of the homogeneous coordinates of the image space. This yields a linear transformation to express

a displacement of E with respect to Σ in terms of the image point:

$$\begin{bmatrix} X \\ Y \\ Z \end{bmatrix} = \begin{bmatrix} (X_4^2 - X_3^2) & -2X_3X_4 & 2(X_1X_3 + X_2X_4) \\ 2X_3X_4 & (X_4^2 - X_3^2) & 2(X_2X_3 - X_1X_4) \\ 0 & 0 & (X_4^2 + X_3^2) \end{bmatrix} \begin{bmatrix} x \\ y \\ z \end{bmatrix}. \quad (3)$$

The ungrounded R-pair in a 2R mechanism is constrained to move on a circle with a fixed centre. The image points that correspond to all possible displacements of the ungrounded link with respect to a fixed reference frame constitute a quadric hyper-surface. If the circle centre has fixed homogeneous coordinates $(X_c : Y_c : Z)$ and radius ℓ_1, the *constraint hyperboloid* in the image space has an equation of the form (Bottema and Roth, 1979):

$$\begin{gathered} 0 = \mathcal{K}_0(X_1^2 + X_2^2)z^2 + (1/4)[\mathcal{K}_0(x^2 + y^2) - 2\mathcal{K}_1xz - 2\mathcal{K}_2yz + \mathcal{K}_3z^2]X_3^2 + \\ (1/4)[\mathcal{K}_0(x^2 + y^2) + 2\mathcal{K}_1xz + 2\mathcal{K}_2yz + \mathcal{K}_3z^2]X_4^2 + (\mathcal{K}_1z - \mathcal{K}_0x)zX_1X_3 + \\ (\mathcal{K}_2z - \mathcal{K}_0y)zX_2X_3 - (\mathcal{K}_0y + \mathcal{K}_2z)zX_1X_4 + (\mathcal{K}_1z + \mathcal{K}_0x)zX_2X_4 + \\ (\mathcal{K}_2x - \mathcal{K}_1y)zX_3X_4, \end{gathered} \quad (4)$$

where $\mathcal{K}_0$ = arbitrary homogenizing constant, $\mathcal{K}_1 = -X_c$, $\mathcal{K}_2 = -Y_c$ and $\mathcal{K}_3 = (X_c^2 + Y_c^2 - \ell_1^2)$.

4. Virtual Platform and Involute Inputs

The three joint input variables are selected to be the change in arclength along the rack due to the change in contact point, given by Δd_i (this choice was made to better suit computations). They are given by the three numbers $\Delta d_i = r\Delta\tau_i$, $i \in \{A, B, C\}$. The $\Delta\tau_i$ are the change between the initial and final rack angles and the pinion radius is r. Because the bases are orthogonal, the change in tangent angle is the same as the change in normal angle: $\Delta\tau_i = \Delta\eta_i$.

To effectively apply the kinematic mapping to workspace analysis, fixed points in E which move on fixed circles in Σ are required. These are supplied naturally when the concept of the *virtual platform* (VP) is employed, see Hayes *et al.* (1998; 1999b). The VP is formed by the triangle whose vertices are the three knee joints expressed relative to the disk frame E: $K_{A/E}$, $K_{B/E}$, $K_{C/E}$ (see Fig. 1). For a given assembly configuration, these *virtual platform points* (VPP) are fixed relative to each other, but change from pose to pose. Next, we require expressions for the VPP in terms of the joint input variables, $\Delta\tau_i$. Consider, for now, only leg A in Fig. 2 and observe that the knee joint K_A, which has a fixed position in the reference frame attached to the rack, R_A, moves on a circle in the fixed frame Σ. But, it also has a relative motion in the moving disk frame E: fix the disk and observe that the relative motion of the rack with respect to E is pure rolling with the

original contact point moving on an involute of the pinion. This gives a complete description (in terms of the change in rack tangent angle) of the motion of the knee joints with respect to both the moving frame, E, and the fixed frame, Σ. Due to their positional dependence on an involute, we call these one parameter sets of knee joint positions *involute inputs*.

The motion of the knee joints of the remaining two legs must be the same type as that of leg A relative to E, but the starting points of the involutes are different. Thus, for every set of three joint input parameters one obtains a set of three VPP expressed in E. With the VPP transformed to involute inputs the kinematic mapping can be used.

The involute inputs were derived in detail in Hayes *et al.* (1999b), but the main steps are described below. Fig. 2 shows the reference coordinate systems used to transform the position of the knee joint from the moving rack reference frame, R_A, to the relatively fixed pinion reference frame, E. The origin of R_A moves along its involute and R'_A gives the new position of R_A after a rotation $\Delta\tau_A$. The intermediate system, E'_A, is fixed relative to E. For each leg, E'_i is rotated from E through $\theta_i = (5\pi/4), (7\pi/4), (\pi/2)$ for $i \in \{A, B, C\}$. Examining Fig. 2, it is easy to see that for each leg the required transformations to take the coordinates of the knee joint K_i from frame R'_i to frame E are (where $c = \cos$, and $s = \sin$)

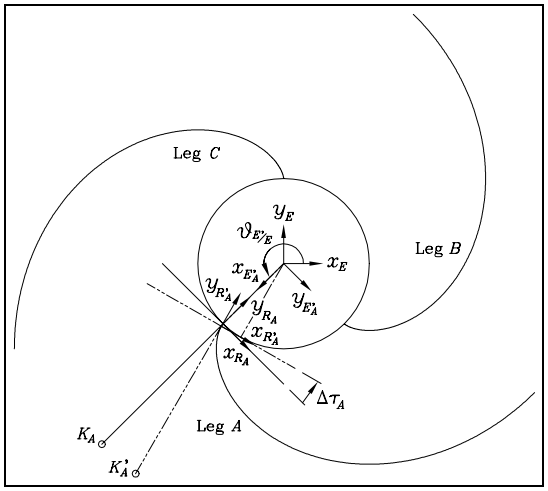

Figure 2. Leg A reference frames.

$$\begin{aligned}\mathbf{T}_{R'_i/E} &= \mathbf{T}_{E'_i/E}\mathbf{T}_{R'_i/E'_i} \\ &= \begin{bmatrix} c\theta_i & -s\theta_i & 0 \\ s\theta_i & c\theta_i & 0 \\ 0 & 0 & 1 \end{bmatrix} \begin{bmatrix} -s\Delta\tau_i & -c\Delta\tau_i & r(c\Delta\tau_i + \Delta\tau_i s\Delta\tau_i) \\ c\Delta\tau_i & -s\Delta\tau_i & r(s\Delta\tau_i - \Delta\tau_i c\Delta\tau_i) \\ 0 & 0 & 1 \end{bmatrix}.\end{aligned}$$

The knee joints, shown in Fig. 1, all have the same coordinates in their respective R_i and R'_i frames:

$$\mathbf{k}_{i/R'_i} = \begin{bmatrix} x_{k_i/R'_i} \\ y_{k_i/R'_i} \\ z \end{bmatrix} = \begin{bmatrix} 0 \\ -\ell_{2_i} \\ 1 \end{bmatrix}.$$

Once the arclength parameters (joint inputs), $\Delta\tau_i$, are given, the coordinates of the knee joints (involute inputs) in frame E, $\mathbf{k}_{i/E}$, are easily determined by left multiplying the $\mathbf{k}_{i/R_i'}$ with the appropriate $\mathbf{T}_{R_i'/E}$,

$$\mathbf{k}_{i/E} \;=\; \mathbf{T}_{R_i'/E}\mathbf{k}_{i/R_i'}. \tag{5}$$

5. Workspace Analysis

For the kinematic analysis it is useful to consider the three sub-chains consisting of a 2R serial leg together with the pinion when the connections to the other two legs have been severed. This means that for a set of joint inputs, $\Delta\tau_i$, one for each leg, substituting the IAC and the input data from Eq. (5) into Eq. (4) gives three constraint hyperboloids in the image space. Note that Eq. (4) covers the case of a point moving on a line ($\mathcal{K}_0 = 0$) which, while of interest for a sub-set of lower-pair jointed planar platforms, is of no interest here. The constraint equation can be simplified by setting $\mathcal{K}_0 = 1$. Also, no platform point should be at infinity, so we can set $z = 1$. Then, cautiously setting $X_4 = 1$, we can rearrange the constraint hyperboloid equation, Eq. (4) (the subscript k_i/E is abbreviated as k):

$$\begin{aligned}\Big(X_1-\tfrac{1}{2}(y_k+\mathcal{K}_2+(x_k-\mathcal{K}_1)X_3)\Big)^2+\Big(X_2-\tfrac{1}{2}((y_k-\mathcal{K}_2)X_3-x_k-\mathcal{K}_1)\Big)^2\\ -\tfrac{\ell_1^2}{4}(1+X_3^2)\;=\;0.\end{aligned} \tag{6}$$

In planes where X_3 is a constant, Eq. (6) represents a circle with centre coordinates

$$\left[\frac{1}{2}(y_k+\mathcal{K}_2+(x_k-\mathcal{K}_1)X_3)\;:\;\frac{1}{2}((y_k-\mathcal{K}_2)X_3-x_k-\mathcal{K}_1)\;:\;X_3\right], \tag{7}$$

and radius

$$R_{X_3} \;=\; \frac{\ell_1}{2}\sqrt{(1+X_3^2)}. \tag{8}$$

The following is a summary of some interesting properties of these image space hyperboloids:

1. The constraint surfaces are skew hyperboloids.
2. The intersection curves with planes $X_3 = const.$ are circles. Points in these planes correspond to positions with fixed orientation.
3. The hyperboloid axes are independent of ℓ_{1_i}. They depend on the relative locations of the fixed base points and of the moving VPP.

By virtue of point 2 above, it is simple to parametrize the constraint hyperboloid by stacking circles, parametrized with the angle ζ, in planes parallel to $X_3 = t =$ a constant. With $-\infty \leq t \leq \infty$ and $0 \leq \zeta \leq 2\pi$, we obtain (note, the axis equations are determined by setting $\ell_1 = 0$):

$$\begin{bmatrix} X_1 \\ X_2 \\ X_3 \end{bmatrix} = \frac{1}{2} \begin{bmatrix} [(x_k - \mathcal{K}_1)t + \mathcal{K}_2 + y_k] + (\ell_1\sqrt{t^2+1})\cos\zeta \\ [(y_k - \mathcal{K}_2)t - \mathcal{K}_1 - x_k] + (\ell_1\sqrt{t^2+1})\sin\zeta \\ 2t \end{bmatrix}. \quad (9)$$

When the knee joint positions for all possible changes in rack tangent angle from Eq. (5) are substituted into Eq. (9), we obtain the family of constraint hyperboloids for a given leg. The solid bounded by the envelope of these hyperboloids is the image of the workspace for that leg when the other two have been disconnected from the pinion. Fig. 3 shows a portion of the solid region for leg A of the platform shown in Fig. 1. There is one envelope corresponding to each leg. The image of the workspace of the entire platform is the solid region bounded by the intersection of these three envelopes. Substituting Eq. (9) into Eq. (3) yields the pre-image of the constraint solid region, i.e., the Cartesian reachable workspace. The pre-image is dependent on the platform reference point (x, y), which we are free to choose. This makes it easy to compute the different Cartesian reachable workspaces of different end-effector reference points. The smallest set of equations is obtained by selecting the origin of E as the reference point.

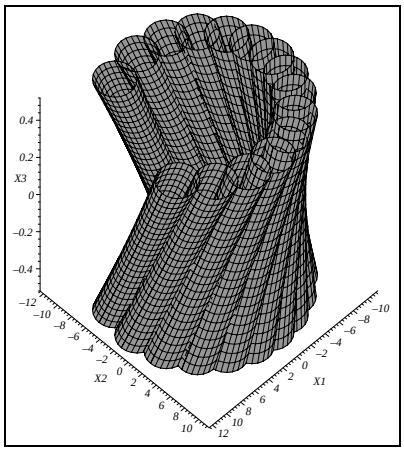

Figure 3. Portion of hyperboloid family.

To obtain the image of the workspace we consider all positions of the end-effector reference point for fixed pinion orientations for each leg. This involves intersecting the envelopes of constraint solids with the planes $X_3 =$ constant. The corresponding curves are envelopes of circles whose radii are given by Eq. (8). We obtain the envelopes for particular values of X_3 by first determining the locus of circle centres. Each envelope is characterized by major and minor parallel offset curves at a distance from the centre locus equal to the hyperboloid circle radius. The respective pre-image is obtained by choosing a platform reference point $(x, y, 1)$ then substituting the expressions for the three envelopes in terms of the $\mathbf{k}_{i/E}$ and (X_1, X_2, X_3, X_4) into Eq. (3). The reachable positions of the pinion reference point for the particular orientation are bounded by the intersections of these six curves. The entire reachable workspace is the union of pre-images of each layer.

6. Example

Table 1 gives the IAC for a manipulator similar to the one shown in Fig. 1, only the link lengths are different, the relative link angles are the same. The $X_{F_i/\Sigma}$ and $Y_{F_i/\Sigma}$ are the coordinates of the base of each leg expressed in the fixed frame, Σ. The initial rack normal angles in the moving frame, E, are $\eta_{i/E}$. The relative angles between the first link and base, and between the second and first links are $\theta_{i_1/0}$ and $\theta_{i_2/1}$, respectively. The location of the contact point along a rack measured in the corresponding rack frame, R_i, is d_{i_3/R_i}. The link lengths, in generic units, are: $r = 2$; $\ell_{i_1} = 6$; $\ell_{i_2} = 12$.

TABLE 1. Initial assembly configuration (IAC).

i	$X_{F_i/\Sigma}$	$Y_{F_i/\Sigma}$	$\eta_{i/E}$	$\vartheta_{i_1/0}$	$\vartheta_{i_2/1}$	d_{i_3/R_i}
A	0	0	225°	90°	315°	0
B	$14\sqrt{2}$	0	315°	90°	45°	0
C	$7\sqrt{2}+6$	$7\sqrt{2}+20$	90°	180°	90°	0

Fig. 4 shows the intersections of the three constraint solid envelopes, obtained after substituting Eq. (5) into Eq. (9), with the plane $X_3 = 0$. Each envelope is pair of parallel transcendental curves, whose characteristics are determined by the corresponding involute. All points bounded by the six curves in this plane, the shaded region in Fig. 4, represent the possible positions of the pinion when it has an absolute orientation of $\varphi = 0$. The pre-image of these curves, obtained after substituting Eq. (9) into Eq. (3), is shown in Fig. 5. The reachable Cartesian workspace of the entire platform for this orientation and reference point is the region bound by all six curves, shown as the shaded area in Fig. 5.

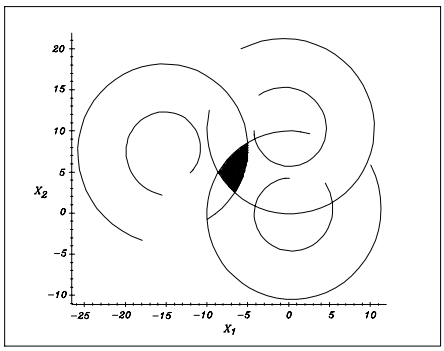

Figure 4. Workspace image for $\varphi = 0$.

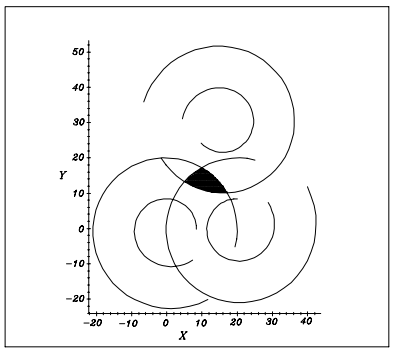

Figure 5. Cartesian Workspace for $\varphi = 0$.

Fig. 6 shows different layers of the reachable Cartesian workspace. There are 13 layers, each representing a 30° increment in the orientation of the pinion. In Fig. 7, the different layers are given different elevations according to the pinion orientation. The top layer is the reachable workspace for a pinion orientation of 180° while the second layer from the bottom is that of −180° orientation. The bottom is the union of all the layers.

The dextrous workspace of a manipulator is usually defined as the set of all points within the reachable workspace that the end-effector can reach with any orientation. Examining Fig. 6 the boundary of the dextrous workspace is seen to be the shaded region that is common to all layers. An area computation reveals that the dextrous workspace comprises 31.71% of the reachable workspace. Moreover, the reachable and dextrous workspace contain no holes; a remarkable result when compared with lower pair jointed three-legged platforms, see Sefrioui and Gosselin (1992; 1995), or Husty (1996), for example.

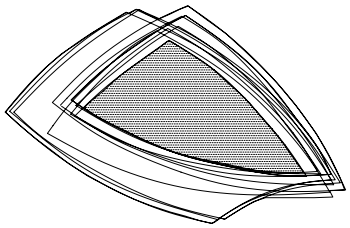

Figure 6. Overlay of workspace layers.

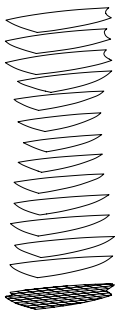

Figure 7. 3D view of workspace layers.

7. Conclusions

In this paper kinematic mapping was used to analyze the workspace of a parallel manipulator. The image of the reachable workspace is a solid region bound by three envelopes of hyperboloids. The pre-image of this solid region, depending on the end-effector reference point, is found by the inverse mapping. The workspace depends on the choice of IAC and reference point. The example shows that these types of platforms can be designed to have a relatively large, hole-free dextrous workspace that is on the order of one-third of the reachable workspace.

8. Acknowledgements

The authors gratefully acknowledge the financial support provided by Professors Paul O'Leary (Institut für Automation, Montanuniversität Leoben)

and Paul Zsombor-Murray (Centre for Intelligent Machines, McGill University). Moreover, they both provided inspiration through lengthy discussions.

References

Agrawal, S.K., Pandravada, R., (1993), Kinematics and Workspace of a Rolling Disk Between Planar Manipulators, *Proc. Am. Control Conf.*, San Francisco, Cal., U.S.A., pp. 741-745.

Bottema, O. and Roth, B., (1979), *Theoretical Kinematics*, Dover Publications, Inc., (1990), New York, N.Y., U.S.A..

Collins, C.L., McCarthy, J.M., (1998), The Quartic Singularity Surface of Planar Platforms in the Clifford Algebra of the Projective Plane, *Mech. Mach. Theory*, vol. 33, no. 7, pp. 931-944.

De Sa, S. and Roth, B., (1981), Kinematic Mappings. Part 1: Classification of Algebraic Motions in the Plane, *ASME, J. of Mech. Design*, Vol. 103, pp. 585-591.

Gosselin, C., (1988), *Kinematic Analysis, Optimization and Programming of Parallel Robotic Manipulators*, Ph.D. thesis, Dept. of Mech. Eng., McGill University, Montréal, Qc., Canada.

Hayes, M.J.D., Zsombor-Murray, P.J., (1998), Inverse Kinematics of a Planar Manipulator with Holonomic Higher Pairs, *Advances in Robotic Kinematics: Analysis and Control*, eds. Lenarčič, J., Husty, M.L., Kluwer Academic Publishers, Dordrecht, pp. 59-68.

Hayes, M.J.D., (1999), *Kinematics of General Planar Stewart-Gough Platforms*, Ph.D. Thesis, Dept. of Mech. Eng., McGill University, Montréal, Canada.

Hayes, M.J.D., Husty, M.L., Zsombor-Murray, P.J., (1999a), Kinematic Mapping of Planar Stewart-Gough Platforms, *Proc. 17th Canadian Congress of Applied Mechanics (CANCAM 1999)*, Hamilton, On., Canada, pp. 319-320.

Hayes, M.J.D., Husty, M.L., Zsombor-Murray, P., (1999b), Solving the Forward Kinematics of a Planar 3-legged Platform With Holonomic Higher Pairs, *ASME Journal of Mechanical Design*, Vol. 121, No. 2, pp. 212-219.

Husty, M.L., (1996), On The Workspace of Planar Three-legged Platforms, *Proc. World Automation Conf., 6th Int. Symposium on Rob. and Manuf. (ISRAM 1996)*, Montpellier, France, Vol. 3, pp. 339-344.

Husty, M.L., Hayes, M.J.D., Loibnegger, H., (1999), The General Singularity Surface of Planar Three-Legged Platforms, *Advances in Multibody Systems and Mechatronics*, Gerhard-Mercator-Universität, Duisburg, Germany, pp. 203-214.

Merlet, J-P., (1990), *Les Robots Parallèles*, Hermès Publishers, Paris, France.

Merlet, J-P., (1996), Direct Kinematics of Planar Parallel Manipulators, *IEEE Int. Conf. on Robotics and Automation*, Minneapolis, U.S.A., pp. 3744-3749.

Merlet, J-P., (1999), *Parallel Manipulators: State of the Art and Perspectives*, http://www-sop.inria.fr/saga/personnel/merlet/merlet.html, Inst. Nat. de Rech. en Inf. et en Auto, France. Dissertation, Stanford University, Stanford, California, U.S.A..

Ravani, B. and Roth, B., (1983), Motion Synthesis Using Kinematic Mappings, *ASME, J. of Mechanisms, Transmissions, & Automation in Design*, Vol. 105, pp. 460-467.

Sefrioui, J., Gosselin, C.M., (1992), Singularity Analysis and Representation of Planar Parallel Manipulators, *Robotics and Autonomous Systems*, vol. 10, pp. 209-224.

Sefrioui, J., Gosselin, C.M., (1995), On the Quadric Nature of the Singularity Curves of Planar Three-Degree-of-Freedom Parallel Manipulators, *Mech. Mach. Theory*, Vol. 30, No. 4, pp. 533-551.